

CERN-TH 2000-232
 IFIC/00-49
 hep-ph/0009053

Monte Carlo simulation for jet fragmentation in SUSY-QCD

V. Berezhinsky^{1,2} and M. Kachelrieß^{3,4}

¹*INFN, Laboratori Nazionali del Gran Sasso, I-67010 Assergi (AQ), Italy*

²*Institute for Nuclear Research, Moscow, Russia*

³*TH Division, CERN, CH-1211 Geneva 23*

⁴*Departament de Física Teòrica, Universitat de València - IFIC/CSIC, Spain*

September 1, 2000

Abstract

We present results from a new Monte Carlo simulation for jet fragmentation in QCD and SUSY QCD for large primary energies \sqrt{s} up to 10^{16} GeV. In the case of SUSY QCD the simulation takes into account not only gluons and quarks as cascading particles, but also their supersymmetric partners. A new model-independent hadronization scheme is developed, in which the hadronization functions are found from LEP data. An interesting feature of SUSY QCD is the prediction of a sizeable flux of the lightest supersymmetric particles (LSPs), if R-parity is conserved. About 10% of the jet energy is transferred to LSPs which, owing to their harder spectra, constitute an important part of the spectra for large $x = E/E_{\text{jet}}$. Spectra of protons and of secondary particles, photons and neutrinos, are also calculated. These results have implications for the decay of superheavy particles with masses up to the GUT scale, which have been suggested as a source of ultrahigh energy cosmic rays.

Key words: Perturbative calculations in QCD, Supersymmetry, Cosmic rays

1 Introduction

QCD, being an essential part of the Standard Model, successfully describes accelerator data for production of hadrons in e^+e^- annihilation and in deep-inelastic scattering. There are two distinctive parts in these calculations: the *perturbative QCD* computation of the parton cascade in jets, and the parton *hadronization*, in which low-virtuality partons are converted non-perturbatively into hadrons.

The QCD parton cascade is usually studied in Modified Leading Logarithmic Approximation (MLLA), where large logarithms, $\ln(Q^2)$ and $\ln(1/x)$, play a crucial role (here Q^2 is the maximum of the perpendicular momentum k_\perp , and $x = k_\parallel/k_\parallel^{\max}$).

This approximation is characterized by remarkable features.

In the MLLA the QCD cascade has a probabilistic interpretation, provided by the absence of interference terms in the tree diagrams. The colour coherence effect is taken into account in the MLLA. It suppresses the emission of soft gluons and results in the Gaussian peak of the parton distribution in terms of $\xi = \ln(1/x)$ (hump-backed plateau).

The evolution of parton cascades in the MLLA (as well as in the LLA) is adequately described by the Dokshitzer–Gribov–Lipatov–Altarelli–Parisi (DGLAP) equations [1].

The parton spectra can be obtained *analytically* and by *Monte Carlo* (MC) simulations.

Examples for analytical solutions are the *limiting spectrum* [2] and the *Gaussian spectrum* [3], in which we include the *distorted Gaussian spectrum* [4, 5]. The limiting spectrum is the most accurate of them. Since we have a special interest in it, we shall shortly review below the basic assumptions under which this solution is obtained.

The limiting spectrum gives the energy spectrum of partons $D_{\text{lim}}(\xi, Y)$ for a given center-of-mass energy \sqrt{s} of an e^+e^- -pair. Here D is the number of cascade partons, $Y = \ln(\sqrt{s}/2\Lambda)$ and Λ is the dimensional QCD scale.

The analytical expression for $D_{\text{lim}}(\xi, Y)$ is given in Refs. [5, 6]. There are two fundamental parameters involved in the limiting spectrum solution: the scale Λ and the minimal virtuality Q_0 of partons, down to which the cascade develops perturbatively; Q_0 can be viewed as the effective mass of the partons. Two assumptions are necessary for the validity of the limiting spectrum. The QCD coupling constant $\alpha_s(k_\perp^2)$ evolves with k_\perp^2 effectively as in the one-loop approximation with three flavors $n_f = 3$ for all k_\perp^2 ,

$$\alpha_s(k_\perp^2) = \frac{12\pi}{(33 - 2n_f) \ln(k_\perp^2/\Lambda^2)}. \quad (1)$$

As a matter of fact, Λ in Eq. (1) is treated in the limiting spectrum solution as a free parameter to fit the e^+e^- -data. The best fit corresponds to $\Lambda = 250 - 270$ MeV. For this range of Λ values, $\alpha_s(M_Z)$, given by Eq. (1) with $n_f = 3$ is in the interval 0.118–0.120, to be compared with the average experimental value $\alpha_s(M_Z) = 0.1184 \pm 0.0031$ [7]. Therefore, the phenomenological parameter Λ coincides well with Λ_{QCD} , which fits the experimental value of $\alpha_s(M_Z)$, in the one-loop approximation with $n_f = 3$.

The second assumption, necessary for the derivation of the limiting spectrum, is $Q_0 = \Lambda$. It gives a reasonable value of Q_0 , but the exact equality of these values has no theoretical justification.

The limiting spectrum solution is valid only for small $x \ll 1$. In this region, which includes the maximal values of multiplicity (in the Gaussian peak), it describes very accurately experimental data at all available energies \sqrt{s} (see, e.g., [8, 9]). The large x up to $x = 1$ give the dominant contribution to the total momentum of cascade partons. Therefore, the limiting spectrum solution does not guarantee that $\int x D_{\text{lim}}(x, s) dx$ precisely equals 2, although it can be valid up to large x [5].

Monte Carlo (MC) simulations of the QCD cascade give a more precise description of the cascade evolution. They are valid for all x including $x \sim 1$. In contrast to the limiting spectrum, in MC simulations one can use $\alpha_s(k_{\perp}^2)$ with the measured value of Λ_{QCD} , varying the number of flavours and two-loop corrections being taken into account. The assumption $\Lambda = Q_0$, specific to the limiting spectrum, is not needed. MC simulations are based on a probabilistic interpretation of the jet cascade. Parton branching is described by the Altarelli–Parisi functions, and the probability of parton evolution between two values of virtualities without branching is given by the Sudakov form factor. Finally, the coherent effect in the soft gluon emission (destructive interference) is conveniently taken into account by angular ordering $\theta_1 > \theta_2 > \theta_3 \dots$ [10], where the indices number the generations (non-ordered processes are suppressed [11]). The first MC simulation with angular ordering was performed in Ref. [10]. At present there are several detailed MC simulations, e.g. [12, 13, 14, 15], which differ mainly in their description of hadronization. We shall now briefly discuss the problem of hadronization.

The description of parton hadronization is based on the assumption of Local Parton–Hadron Duality (LPHD) [16]. This hypothesis implies that when Q_0 is small enough (of the order of Λ) there is a proportionality between the spectra of partons and hadrons, with relations between their momenta, which are local in the phase space. Such an interpretation can be justified by the idea of preconfinement [17].

As far as spectra are concerned, LPHD implies a proportionality between the hadron and parton spectra. In Refs. [5, 6], it is emphasized that, most reasonably, this proportionality holds not on a “one parton – one hadron” basis, but for the number of particles averaged over a finite interval $\Delta\xi \sim 1$.

The LPHD hypothesis for limiting spectrum straightforwardly results [5] in

$$D_{\text{had}}(x, \sqrt{s}) = K_h(Q_0) D_{\text{part}}(x, \sqrt{s}, Q_0), \quad (2)$$

where the constant K_h is universal, in the sense that it does not depend on \sqrt{s} .

Equation (2) completes our description of the limiting spectrum, expressing the hadron spectrum through the spectrum of partons. The constant K_h , which connects the two spectra, is found from a comparison with experimental data as $K_h \approx 1.3$ for $\Lambda = Q_0 \approx 270$ MeV [8], and it does not change with energy unless some new physics (e.g. supersymmetry) appears.

In MC simulations, the parameter Q_0 is in principle a free parameter found by fitting experimental data. For HERWIG [12] and PYTHIA [13], for example, $Q_0 \sim 1$ GeV. Several detailed hadronization models are used in simulations, e.g. the independent fragmentation model, the Lund string model [18], and the cluster fragmentation model [19]. Usually, these models use many free parameters and require to keep track of the four-momentum evolution of all partons.

The calculations described above are valid up to $\sqrt{s} \sim 1\text{--}10$ TeV. At higher energies the production of supersymmetric particles is expected to change the results.

One might be interested in much higher energies, being inspired by the production of superheavy particles up to the GUT scale in the Universe. Such particles can be produced by topological defects and by many processes at the post-inflationary stage of the Universe. Recently superheavy particles with masses $M_X \sim 10^{12}\text{--}10^{14}$ GeV attracted much attention as a source of the observed Ultra High Energy Cosmic Rays (UHECR) with energies $10^{19}\text{--}10^{20}$ eV (for recent reviews, see [21]).

The limiting spectrum for SUSY QCD was calculated in Ref. [22] for very high energies \sqrt{s} , corresponding to masses of superheavy particles $M_X \sim 10^{12}\text{--}10^{14}$ GeV. The supersymmetric partons (squarks and gluinos or jointly spartons) participate in the cascade until the virtualities t of the particles drop below the mass scale of SUSY particles, $t \sim M_{\text{SUSY}}^2$. Then a SUSY particle decays, producing in the end the Lightest Supersymmetric Particle (LSP), for which the lightest neutralino is usually considered. The role of supersymmetric partners is two-fold: they double the number of parton types in the cascade, and they change the evolution of $\alpha_s(k_\perp^2)$. Even at small $t \ll M_{\text{SUSY}}^2$, the cascade remembers the number of flavours at large t because, for example, each squark leaves after its decay a quark, which continues QCD cascading. At large t and small $x \ll 1$ gluons and gluinos dominate and their “children” constitute the dominant part of the cascade at small t . Therefore, the dominant contribution to the limiting spectrum is given by gluons and gluinos.

The SUSY QCD limiting spectrum solution has two drawbacks with respect to ordinary QCD. First, the number of flavours that determine the evolution of the coupling constant according to Eq. (1) has to be fixed to *one* value of n_f for the whole range of k_\perp^2 . Second, the limiting spectrum for ordinary QCD is normalized by experimental data, which are absent in the case of SUSY QCD. Normalization due to the conservation of momentum $\int x D_{\text{lim}}(x, s) dx = 2$ is unreliable, since the limiting spectrum is not valid for large x , which give the main contribution to the integral (see discussion in [22]).

During the last few years, the production and decays of supersymmetric particles have been included in most MC simulations focusing on LHC studies. Although the LHC will operate above the expected threshold of SUSY particle production, its energy is not large enough for these particles to participate in the QCD cascade. Therefore, all currently available MC simulations consider only on-shell decays of spartons and neglect possible branchings of gluinos and squarks¹. Another obstacle against the use of standard MC simulations at extremely large energies around $\sqrt{s} \sim 10^{12} - 10^{14}$ GeV is that the necessary numerical precision and the required amount of memory space and computing time become a challenge for present-day computers.

We have therefore developed a new MC simulation, which includes as cascading particles not only gluons and quarks but also gluinos and squarks. We consider cascades that are initiated by the decay to two jets of superheavy particles with mass $M_X \sim 10^{12}\text{--}10^{14}$ GeV, or by e^+e^- annihilation at $s = M_X^2$. SUSY partons, squarks and gluinos, are produced in the fragmentation of ordinary partons and vice versa. All squarks and gluinos are assumed to have equal masses, for which we use $M_{\text{SUSY}} = 200$ GeV and $M_{\text{SUSY}} = 1000$ GeV. When the virtuality of the cascading particles drops below M_{SUSY}^2 , spartons decay to LSPs (neutralinos), which freely escape. The perturbative development of the cascade continues with ordinary partons until their virtualities reach Q_0^2 , for which we use $Q_0^2 = 0.625$ GeV² to

¹The future C++ version of HERWIG will include branchings of spartons [23].

fit the data at small energies \sqrt{s} . We use a new hadronization procedure. It is based on a model-independent, phenomenological approach, in which hadronization functions for large s (or M_X) are calculated from hadron spectra observed at small s (M_X). This method can be used for any type of hadrons as well as for photons and neutrinos, if their spectra are known with good enough accuracy at small energy.

Following Ref. [20], we shall use the following notation:

Λ is the dimensional QCD scale,

$Y = \ln(\sqrt{s}/2\Lambda)$,

$t = p_\mu^2$ is the virtuality of cascade partons,

$Q^2 = t_{\max}$ is the virtuality of the primary parton,

Q_0^2 is the minimum virtuality of the perturbative evolution of the QCD cascade,

$z = E'/E$, where E and E' are the energies of ingoing and outgoing partons at fragmentation,

$\zeta = 1 - \cos \theta$, where θ is the angle between two outgoing partons,

$\tilde{t} = \zeta E^2$,

k_\perp, k_\parallel are the transverse and parallel momenta transferred, respectively,

$x = k_\parallel/k_\parallel^{\max}$,

$\xi = \ln(1/x)$.

2 MC Simulation of the Perturbative Phase of SUSY QCD Cascades

The perturbative part of our simulation is very similar to those of MCs for ordinary QCD cascades, except for including spartons and the condition for their exit from the cascade. We consider a superheavy X particle with mass M_X which decays into two jets with energy $E_{\text{jet}} = M_X/2$. We assume that the primary partons produced in the X particle decay have the maximum virtuality $Q^2 = m_X^2/4$ and that the X particle has equal branching ratios to all partons. As to the first assumption, in reality, there is a distribution of partons with different t , but the Sudakov form factors suppress small t values. The second assumption is made because of the unspecified interactions of the X particles.

Our simulation closely follows the angular ordered parton cascade algorithm developed in Refs. [10, 19]. It is convenient to use in this algorithm the variable $\tilde{t} = \zeta E^2$, where E is the energy of the incoming parton, $\zeta \approx 1 - \cos \theta$, and θ is the angle between the two emitted partons. A primary parton with energy E_{jet} ($= m_X/2$) and angular variable $\xi_0 \leq 1$ initiates a cascade, which proceeds until the ordinary partons reach the minimal virtuality $\tilde{t} = 4Q_0^2$. Here the perturbative evolution of the cascade terminates.

In each branching of an incoming parton i with \tilde{t}' , we generate with the veto algorithm [24] a new \tilde{t} and z according to the probability distribution

$$d\mathcal{P}_i(\tilde{t}, z) = \sum_{jk} \frac{d\tilde{t}}{\tilde{t}} \frac{dz}{2\pi} \alpha_s \left[z^2 (1-z)^2 \tilde{t} \right] P_{i \rightarrow jk}(z) \frac{\Delta_i(\tilde{t}')}{\Delta_i(\tilde{t})}. \quad (3)$$

Here, the sum includes all possible branching channels jk , $z^2(1-z)^2\tilde{t}$ is the parton transverse momentum, and Δ_i is the product of the individual Sudakov-like form

factors $\Delta_{i \rightarrow jk}$ [19] ,

$$\Delta_{i \rightarrow jk}(\tilde{t}) = \exp \left[- \int_{4\tilde{t}_{\min}}^{\tilde{t}} \frac{dt'}{t'} f_{i \rightarrow jk}(t') \right] \quad (4)$$

with

$$f_{i \rightarrow jk}(\tilde{t}) = \int_{z_{\min}}^{z_{\max}} \frac{dz}{2\pi} \alpha_s \left[z^2(1-z)^2 \tilde{t} \right] P_{i \rightarrow jk}(z). \quad (5)$$

The unregularized Altarelli–Parisi splitting functions $P_{i \rightarrow jk}(z)$ of SUSY QCD [26] are given in Table 1.

The angular ordering $\zeta_j, \zeta_k < \zeta_i$ for the branching $i \rightarrow jk$, which takes into account colour coherence, is equivalent to $\tilde{t}_j < z^2 \tilde{t}_i$ and $\tilde{t}_k < (1-z)^2 \tilde{t}_i$. These conditions result in

$$z_{\min} = \sqrt{\tilde{t}_{\min}/\tilde{t}}, \quad z_{\max} = 1 - \sqrt{\tilde{t}_{\min}/\tilde{t}}. \quad (6)$$

For the evolution of the running coupling α_s as a function of gluon virtuality t at small momentum transfer $t < t_{\text{SUSY}}$, we use the standard two-loop dependence with variable n_f and thresholds, and normalize α_s as $\alpha_s(M_Z) = 0.119$, which corresponds to $\Lambda_{\overline{MS}}^{(5)} = 222$ MeV. At large momentum transfer $t > t_{\text{SUSY}}$ we use minimal SUSY-SU(5) coupling constant evolution [25], normalizing the coupling constant at $\sqrt{t} = M_{\text{GUT}} = 1 \cdot 10^{16}$ GeV, as $\alpha_s(M_{\text{GUT}}^2) \approx 1/25.8$. Explicitly we use

$$\alpha_s(t) = \frac{\alpha(M_{\text{GUT}}^2)}{1 + b_s/(4\pi) \ln(t/M_{\text{GUT}}^2) \alpha(M_{\text{GUT}}^2)}, \quad (7)$$

where $b_s = 9 - n_f$ is a constant, that governs the evolution of the coupling constant with t . At $t > t_{\text{SUSY}}$, $n_f = 6$ and $b_s = 3$. The above assumption means that we introduce, instead of many thresholds corresponding to SUSY particles with different masses, a single threshold at $t = t_{\text{SUSY}}$. This is a reasonable thing to do in view of the large uncertainties in our knowledge of mass spectrum of SUSY particles. Equation (7) approximates accurately enough the evolution of $\alpha_s(t)$ as calculated in Ref. [27], when $t_{\text{SUSY}} \approx 2 \cdot 10^5$ GeV². Starting from this value, $\alpha_s(t)$ evolves in the regime of Eq. (7). Note that t_{SUSY} does not necessarily coincide with the scale M_{SUSY} , the universal mass of squarks and gluino, for which we use as two representative values $M_{\text{SUSY}} = 200$ GeV and $M_{\text{SUSY}} = 1$ TeV. In particular, the low value of t_{SUSY} used here is compatible with much larger M_{SUSY} , as emphasized in Ref. [27].

Finally, we have to specify the value of the cut-off \tilde{t}_{\min} for the cascade evolution. We do not distinguish between different quark flavours and use $\tilde{t}_{\min} = 0.625$ GeV² for all branchings in which only ordinary particles are produced and $\tilde{t}_{\min} = M_{\text{SUSY}}^2$, where M_{SUSY} is the typical mass scale of the spartons, for branchings in which SUSY particles are produced, respectively.

Let us now describe a step $i \rightarrow jk$ in our simulation. For an incoming parton i with \tilde{t} we generate first a new cascade variable \tilde{t} , according to the probability distribution given by the ratio $\Delta_i(\tilde{t}')/\Delta_i(\tilde{t})$. Then we select the branching channel jk using as weight $f_{i \rightarrow jk}(\tilde{t})$ and generate z according to the probability distribution $\alpha_s [z^2(1-z)^2 \tilde{t}] P_{i \rightarrow jk}(z)$.

The last ingredient in the perturbative part of our simulation is the exit of supersymmetric particles from the cascade. We assume that the neutralino $\tilde{\chi}$ is the

LSP and that R-parity is conserved. Reaching $\tilde{t}_{\min} = M_{\text{SUSY}}^2$, squarks and gluinos decay as $\tilde{q} \rightarrow q + \tilde{\chi}$ and $\tilde{g} \rightarrow q + \bar{q} + \tilde{\chi}$, thus producing UHE LSPs.

In fact, we are running in this work two Monte Carlo simulations: with the ordinary QCD and with SUSY QCD.

In the former case supersymmetric partons are not included, and for perturbative calculations we assume the SM particle content with $\alpha_s(t)$ evolution in two-loop approximation with proper thresholds. We fix $Q_0^2 = 0.625 \text{ GeV}^2$. We need these calculations mostly to test our method.

The assumptions of SUSY QCD Monte Carlo are described above. At $\tilde{t}_{\min} < M_{\text{SUSY}}^2$ cascade develops according to ordinary QCD scheme.

3 Hadronization

The Monte Carlo simulation described in the last section is completely determined by perturbative physics. How the spectrum of coloured quarks and gluons $D_i(x, \sqrt{s})$ is transformed into the spectrum of hadrons $D_{\text{had}}(x, \sqrt{s})$ is still an open problem. Monte Carlo simulations have to use some hadronization model (see Introduction), which describes the non-perturbative evolution of the cascade for $\tilde{t} < 4\tilde{t}_{\min}$. Two hadronization models, the cluster fragmentation model [19] used in HERWIG [12] and the Lund string model [18] used in PYTHIA [13], require the knowledge of the four-momenta of all the partons. Thus these models need detailed time and memory-consuming computations.

We suggest here a phenomenological, model-independent hadronization scheme based on the knowledge of the hadron spectra at energies \sqrt{s} smaller than the energy of interest. This method is valid for any hadron type and can be applied to the secondary particles, such as photons and neutrinos, as well. The application of this method is somewhat restricted (e.g. it cannot give the angular distribution of particles in a jet or correlations), but its use is very efficient for the decay of superheavy particles, where multiplicity, and hence the number of partons to follow in a simulation is very large.

Our hadronization scheme depends on only one theoretical assumption, which is reliable and testable. Namely, we assume that the unknown non-perturbative physics can be factorized into hadronisation functions $f_i(z)$ that do *not* depend on \sqrt{s} ,

$$D_h(x, \sqrt{s}) = \sum_{i=q,g} \int_x^1 \frac{dz}{z} D_i(x/z, \sqrt{s}) f_i^h(z), \quad (8)$$

where the index h runs through different types of hadrons, e.g. π^0, π^\pm, N etc.

The functions $f_i^h(z)$ give the probability that a parton i with energy E is converted into a hadron h with energy zE . It is implicitly assumed in Eq. (8) that the perturbative cut-off Q_0 is fixed, and f_i^h is determined for this value of Q_0 , although in principle for every Q_0 and $D_i(x, \sqrt{s}, Q_0)$ one can find $f_i^h(z, \sqrt{s}, Q_0)$ to fit the observed hadron spectra.

Equation (8) with energy independent hadronization functions follows from basic principles and is confirmed (see below) at energies of e^+e^- colliders. It has the form of a Volterra integral equation of the first kind though in contrast to the standard case, the RHS contains not one but two unknown functions f_i for every h . In principle, the two functions $f_g(x)$ and $f_q(x)$ can be uniquely determined if D_h is

known as an analytic function without errors for two different values of \sqrt{s} . In practice, $D_h(x)$ is known only as a discrete set of experimental data and Eq. (8) represents an ill-posed inversion problem² [29]. Instead of solving Eq. (8) by an inversion method, we prefer to find physically motivated trial functions for f_i to fit the experimental data at $\sqrt{s} = 91.2$ GeV.

In terms of the more convenient variable $\xi = \ln(1/x)$, Eq. (8) has the form

$$D_h(\xi, \sqrt{s}) = \sum_{i=q,g} \int_0^l d\xi' D_i(\xi - \xi', \sqrt{s}) f_i(\xi'), \quad (9)$$

where the index h in the hadronization functions is suppressed.

In the limiting spectrum, when $Q_0 = \Lambda$, the hadronization functions f_i are proportional to delta functions. Inspired by this analytical solution we choose for f_i Gaussian functions,

$$f_i(\xi) = a_i \exp\left(-\frac{(\xi - \xi_{\max,i})^2}{\sigma_i^2}\right). \quad (10)$$

With this hadronization function the approximate proportionality holds between spectra of partons and hadrons as LPHD demands. The position of the peak in the hadronization function determines the shift between the maxima of parton and hadron spectra. While for gluons the hadronization function $f_g(\xi)$ should vanish for $\xi \rightarrow 0$, because gluons have to split their energy to a $q\bar{q}$ pair, for quarks $f_q(\xi)$ can be finite at $\xi = 0$.

The hadronization functions we obtained for $Q_0^2 = 0.625$ GeV² from a fit to LEP data at $\sqrt{s} = 91.2$ GeV are shown in Fig. 1.

Our hadronization scheme has been tested by two methods: for relatively small energies, $\sqrt{s} = 58$ GeV and 133 GeV, we confronted our calculations with LEP data, and for very large \sqrt{s} (or M_X) we compared the calculated spectrum with the limiting spectrum, using a special case when it is correct (see below). In both cases ordinary QCD Monte Carlo was used.

Figures 2-4 display a comparison between the charged hadron spectrum from our MC simulation for ordinary QCD and experimental data [28] at $\sqrt{s} = 58, 91.2$ and 133 GeV, respectively.

Let us now discuss whether the hadronization functions $f_i(\xi)$ found from the fit to data at $\sqrt{s} = 91.2$ GeV can really be used at $M_X = 10^{12}$ – 10^{16} GeV.

First of all we note, that a test can be given by LPHD, which demands approximate proportionality between parton and hadron spectra. It implies that the ξ' values, that give the dominant contribution to the integral in Eq. (9), are about the same at $\sqrt{s} = 91.2$ GeV and at large M_X . Numerical tests show that this is indeed the case for both the quark and the gluon contribution.

As a critical test of our hadronization scheme, we compared the limiting spectrum with the results of our simulation for a special, well-controlled case of ordinary QCD with the number of quark flavours $n_f = 3$, and with $\alpha_s(k_\perp^2)$ given by

²Volterra integral equations of the first kind can be solved normally by linearization, even if the LHS are data. However, the lower integration limit in (8) does not represent a sharp cut-off because the kernels $D_i(x)$ vanish for $x \rightarrow 1$. Therefore, Eq. (8) behaves effectively like a Fredholm equation, and these are known to be extremely ill-conditioned.

Eq.(1). For the limiting spectrum in this case we can use the normalization constant $K_h \approx 1.3$ obtained by fitting experimental data [9]. Since we do not introduce new high-energy physics, the limiting spectrum is valid for any initial energy M_X (see Introduction). In Fig. 5, we show the ratio of these two (charged) hadron spectra. The agreement between the two spectra is excellent, except for the small $\xi \lesssim 6$ region where it is known that the limiting spectrum is not valid. The disagreement reaches 50% at $\xi \approx 2.1$ ($x \approx 0.12$).

In conclusion, we think that our hadronization recipe is a valid alternative to the extrapolation of the Lund string or the cluster fragmentation model to extremely large M_X .

4 Results: Spectra of Hadrons and Secondary Particles

Using the algorithm for the perturbative evolution of the SUSY QCD cascade as described in Section 2 and our hadronization scheme from Section 3, we can now compute the fragmentation spectra of hadrons. As numerical values for M_X , we choose in the graphs given as examples three values interesting for UHECR physics, $M_X = 10^{12}, 10^{13}, 10^{14}$ GeV, as well as $M_X = 10^6$ and 10^{16} GeV as lowest and highest scale of interest. Similarly, we use $M_{\text{SUSY}} = 200$ GeV and $M_{\text{SUSY}} = 1000$ GeV as two representative values for the SUSY mass scale.

In Figs. 8 and 9, the hadron spectra $dN_{\text{had}}/d\xi$ from SUSY QCD MC simulations are displayed as function of ξ for $M_{\text{SUSY}} = 200$ GeV and $M_{\text{SUSY}} = 1000$ GeV, respectively; in both figures the spectra were calculated for $M_X = 10^{12}, 10^{13}, 10^{14}$ GeV. For the GUT scale $M_X = 10^{16}$ GeV, the hadron spectra $dN_{\text{had}}/d\xi$ are shown in Fig. 10 and for the low scale $M_X = 10^6$ GeV in Fig. 11. *The hadron spectra depend only weakly on M_{SUSY} , with increasing differences for larger values of M_X .* Both effects are easy to understand: when spartons disappear from the cascade at $\tilde{t} \sim M_{\text{SUSY}}^2$ due to on-shell decays, each of them leaves there an ordinary parton with similar virtuality. Therefore, the cascade proceeds as if nothing had happened, except that some energy is lost through the emission of neutralinos and leptons, which is not large ($\sim 10\%$). Second, the importance of spartons for the cascade decreases for smaller values of M_X , thereby reducing also the dependence of the hadron spectra on M_{SUSY} for smaller M_X .

The weak dependence of the spectra on M_{SUSY} justifies our choice of an universal value for the masses of supersymmetric particles. Indeed, if we assume now that supersymmetric particles have different masses in the range 200-1000 GeV, the resulting hadron spectra will differ less than in Figs. 10 and 11.

The signature of supersymmetry in decays of superheavy X particles is the production of LSPs, which we assume as stable neutralinos. They are generated in the cascade mostly when the virtuality of the spartons approaches M_{SUSY}^2 . The calculated neutralino spectra are shown in Figs. 12–15 for the same parameters as the hadron spectra in Figs. 8–11. Like the hadron spectra, they have the characteristic Gaussian form, however with a shifted position of their maxima due to their larger cut-off M_{SUSY} in the shower development. The energy fraction taken away by the neutralinos is typically 10% for values of M_X interesting for UHECR physics, with

a minimum of 5% for $M_X = 10^6$ GeV and $M_{\text{SUSY}} = 1$ TeV and a maximum of 12% for $M_X = 10^{16}$ GeV and $M_{\text{SUSY}} = 200$ GeV.

We have only derived a common hadronization function for all hadrons and, consequently, we cannot calculate directly, e.g. pion or nucleon spectra through Eq. (8). Since the fraction of energy ϵ_i going into different meson and baryon species is determined by the non-perturbative process of hadronization, these fractions as the hadronization functions themselves do not depend on s . Thus, we can use the value from Z decay, $\epsilon_N \approx 0.05$ and $\epsilon_\pi \approx 0.95$. Then

$$\frac{dN_{\text{nucl}}}{dx} = \epsilon_N \frac{dN_{\text{had}}}{dx}, \quad \frac{dN_\pi}{dx} = \epsilon_\pi \frac{dN_{\text{had}}}{dx}. \quad (11)$$

Using the hadron spectra obtained in the last Section, it is simple to calculate analytically the spectra of secondary particles, photons and neutrinos. The normalized photon spectrum from a decay of one X particle at rest is given by

$$\frac{dN_\gamma}{dx} = \frac{2}{3} \epsilon_\pi \int_x^1 \frac{dy}{y} \frac{dN_{\text{had}}}{dy}. \quad (12)$$

The total neutrino spectrum, given by the sum from decays of pions and muons, can be presented in the following form,

$$\frac{dN_\nu}{dx} = \frac{2}{3} \epsilon_\pi \left(\frac{dN_{\nu_\mu}}{dx} (\pi \rightarrow \mu \nu_\mu) + \frac{dN_{\nu_\mu}}{dx} (\mu \rightarrow \nu_\mu \nu_e e) + \frac{dN_{\nu_e}}{dx} (\mu \rightarrow \nu_\mu \nu_e e) \right), \quad (13)$$

where for pion decay

$$\frac{dN_{\nu_\mu}}{dx} (\pi \rightarrow \mu \nu_\mu) = R \int_{Rx}^1 \frac{dy}{y} \frac{dN_{\text{had}}}{dy} \quad (14)$$

and for muon decay

$$\frac{dN_{\nu_i}}{dx} (\mu \rightarrow \nu_\mu \nu_e e) = R \int_x^1 \frac{dy}{y} \int_y^{y/r} \frac{dy'}{y'} \frac{dN_{\nu_i}}{dy} \frac{dN_{\text{had}}}{dy'}, \quad (15)$$

with

$$\frac{dN_{\nu_e}}{dy} = 2 - 6y^2 + 4y^3, \quad \frac{dN_{\nu_\mu}}{dy} = \frac{5}{3} - 3y^2 + \frac{4}{3}y^3, \quad (16)$$

and $r = (m_\mu/m_\pi)^2$, $R = 1/(1 - r)$.

The resulting nucleon, photon and neutrino spectra $x^3 dN_i/dx$ are shown as functions of x together with the spectra of neutralinos in Fig. 17 for $M_{\text{SUSY}} = 200$ GeV and $M_X = 10^{12}$ GeV and $M_X = 10^{14}$ GeV, respectively. We have multiplied the spectra by x^3 in order to facilitate the comparison of our spectra with the energy spectra of observed UHECR. At $x \gtrsim 0.7$, the spectra have some uncertainties because of the unknown branching ratios of the X particle into (s)partons and fluctuations due to the small number of produced particles. The excess of nucleons over secondary particles, neutrinos and gamma, at largest x is a result of kinematical effect and the steep spectra of pions and nucleons in the end of the spectrum.

5 Discussion

In this Section we compare for large M_X the results of our MC for the two cases, SUSY QCD and ordinary-QCD, with other computations, and most notably with limiting spectrum calculations. The latter case of ordinary QCD is formally a special case of our MC simulation for SUSY QCD in the limit $M_{\text{SUSY}}, t_{\text{SUSY}} \rightarrow \infty$, i.e. α_s is given by two-loop approximation with variable n_f , and the probability to produce a sparton is zero.

The validity of our method has been proved by the tests described in Section 3. If no new physics beyond the three light quark flavours is introduced, the k_\perp -dependence of α_s is given by Eq. (1) with $n_f = 3$ and the limiting spectrum with $K_h = 1.3$ is valid for arbitrary high energies. We can calculate the hadron spectrum in our ordinary QCD MC (hadronization procedure included), introducing there the same assumptions about n_f and α_s . The excellent agreement is illustrated by Fig. 5. The disagreement seen at large x is natural, because the limiting spectrum is not valid there.

It is instructive to compare our MC for ordinary QCD with variable n_f and the exact behaviour of $\alpha_s(k_\perp)$ with the limiting spectrum with fixed number of flavours $n_f = 3$ and $n_f = 6$. It is clear that, in neither case, $\alpha_s(k_\perp)$ from Eq. (1) describes correctly α_s in the whole interval of k_\perp , and the MC spectrum should be between these two solutions. Figures. 6 and 7 show that this is indeed the case. The accuracy of each limiting spectrum compared with the MC spectra is better than 30–50%.

In Ref. [30], HERWIG was used to obtain fragmentation spectra in case of ordinary QCD. The maximal mass M_X possible to simulate was $M_X = 10^{11}$ GeV and even for this not very large value of M_X the computations required several months. The spectra were displayed only for large $x > 0.01$, beyond the Gaussian peak. One of the conclusions of this work was that at $x \geq 0.2$ the proton yield is higher than the photon and neutrino yield. However, it was later realized that this result is caused by the tendency of HERWIG to overproduce protons at large x (Ref. [31], see also [33]).

Let us come over to our SUSY QCD MC and compare the simulated spectra with the SUSY limiting spectrum [22]. The spectra disagree both in the position of the Gaussian peak and in its height. To clarify which assumptions of the SUSY QCD limiting spectrum are responsible for this disagreement, we re-run the SUSY QCD MC simulation with a set of assumptions as similar as possible to those used in the derivation of the SUSY QCD limiting spectrum. We found that the main reason for the disagreement is the universal dependence of $\alpha_s(t)$, taken as $\alpha_s^{-1}(t) = (b_s/4\pi) \ln(t/\Lambda^2)$, with $b_s = 3$ for SUSY, together with $\Lambda = Q_0 = 250$ MeV. It differs from α_s with a variable number of flavours, which is used in SUSY QCD MC, by a factor 1.4–3 in the whole k_\perp^2 range, with largest disagreement at small k_\perp . Changing the evolution of $\alpha_s(k_\perp)$, an agreement can be reached between the MC and the SUSY QCD limiting spectrum: we run the SUSY QCD MC including only gluons and (massless) gluinos with fixed $b_s = 3$ and with frozen $\alpha_s(\tilde{t})$ for $\tilde{t} < 0.9 \text{ GeV}^2$, which is a reasonable physical assumption. The comparison with the SUSY QCD limiting spectrum for partons is shown in Fig. 16. The two spectra agree indeed quite well.

An interesting alternative approach to computing the fragmentation spectra produced by decays of superheavy particles was suggested in a recent work [31]. In this method, the event generator SPYTHIA [32] was used to simulate fragmentation

spectra of partons and spartons into protons, photons, and neutrinos at the scale $M_X = 10^4$ GeV. Then the DGLAP equations were used to evolve the fragmentation functions up to the scale 10^{12} – 10^{13} GeV.

It is premature to compare our results, since in [31] preliminary results are presented, but the spectra, as displayed in [31] and [33], do not agree well with ours. In particular, the Gaussian peak is broader than in our calculations, Fig. 17. Comparing these spectra one should be aware of the differences in methods and assumptions. For example, we treat spartons as cascading particles, while in SPYTHIA spartons are taken as on-shell particles, which decay but do not cascade. On the other hand, the SPYTHIA spectrum is used only as the input, and the evolution to higher energies includes cascading. This difference will be eliminated with the C++ version of HERWIG [23], which will be available soon.

6 Summary

We have developed a new MC simulation for jet fragmentation in ordinary QCD and SUSY QCD, which is valid for initial energies up to the GUT scale. The simulation includes a perturbative part, operating at virtualities higher than the infrared cut-off $Q_0^2 = 0.625$ GeV, and a hadronization part.

The perturbative part for SUSY QCD includes squarks and gluinos as cascade particles with a universal mass M_{SUSY} . The evolution of $\alpha_s(t)$ takes into account the correct number of active flavours and spartons at a given t . The influence of the scale M_{SUSY} on the hadron spectrum is rather weak for the studied range $300 \leq M_{\text{SUSY}} \leq 1000$ GeV. It implies that if supersymmetric particles have different masses in the range 200 -1000 GeV, the resulting difference in the hadron spectra remains small (see Section IV and Figs. 10 and 11).

The hadronization scheme is model-independent and based on the well justified and tested assumption that the hadronization function $f_i^h(z)$, see Eq. (8), does not depend on \sqrt{s} . Thus the hadronization function could be calculated from LEP data. Our scheme was tested at $\sqrt{s} = 58$ and 133 GeV against experimental data and for very large values of M_X by a comparison with the limiting spectrum solution for ordinary QCD. For the aim of this comparison, we calculated hadron spectra using the MC for ordinary QCD in the case when the limiting spectrum is known to be correct: $n_f = 3$ and $\alpha_s(t)$ given by Eq. (1). The excellent agreement between both spectra is illustrated by Fig. 5.

The spectra of nucleons and secondary particles, photons, neutrinos, as well as neutralinos, have been calculated and presented in Fig. 17. These spectra can be used for calculations of fluxes of ultra high energy cosmic rays, produced by superheavy dark matter and by topological defects.

Acknowledgments

We acknowledge with gratitude the participation of R. Sang in the initial stage of this work. We are grateful to Yu.L. Dokshitzer, V.A. Khoze, S.S. Ostapchenko and B.R. Webber for many useful explanations and comments. MK would like to thank the Alexander von Humboldt-Stiftung for a Feodor-Lynen grant and the EC for

a Marie-Curie grant. The work of MK was partially also supported by DGICYT grant PB95-1077 and by the EC under the TMR contract ERBFMRX-CT96-0090. The work by VB was performed within INTAS Project No 99-01065.

References

- [1] V.N. Gribov and L.N. Lipatov, Sov. J. Nucl. Phys. **15**, 438 and 675 (1972); G. Altarelli and G. Parisi, Nucl. Phys. **B126**, 298 (1977); Yu.L. Dokshitzer, Sov. Phys. JETP **46**, 641 (1977).
- [2] Yu.L. Dokshitzer and S.I. Troyan, Leningrad preprint, LNPI-922 (1984); Ya.I. Azimov, Yu.L. Dokshitzer, V.A. Khoze and S.I. Troyan, Z. Phys. **C27**, 65 (1985), *ibid.* **C31**, 213 (1986).
- [3] A.H. Mueller, Proc. 1981 Int. Symp. on Lepton and Photon Interactions, ed. W. Pfeil, Bonn, 689 (1981); Yu.L. Dokshitzer, V.S. Fadin and V.A. Khoze, Phys. Lett. **B115**, 242 (1982).
- [4] C.P. Fong and B.R. Webber, Phys. Lett. **B229**, 289 (1989), Nucl. Phys. **B355**, 54 (1991).
- [5] Yu.L. Dokshitzer, V.A. Khoze, A.H. Mueller, and S.I. Troyan, *Basics of Perturbative QCD*, Editions Frontières 1991.
- [6] V.A. Khoze and W. Ochs, Int. J. Mod. Phys. **A12**, 29149 (1997).
- [7] S. Bethke, J. Phys. **G26**, R27 (2000).
- [8] V.A. Khoze, S. Lupia and W. Ochs, Phys. Lett. **B386**, 451 (1996).
- [9] S. Lupia and W. Ochs, Eur. Phys. J. **C2**, 307 (1998).
- [10] G. Marchesini and B.R. Webber, Nucl. Phys. **B238**, 1 (1984).
- [11] A.H. Mueller, Phys. Lett. **B104**, 161 (1981); B.I. Ermolaev and V.S. Fadin, JETP Lett. **33**, 269 (1981); A. Bassetto, M. Ciafaloni, G. Marchesini and A.H. Mueller, Nucl. Phys. **B207**, 189 (1982); Yu.L. Dokshitzer, V.S. Fadin and V.A. Khoze, Phys. Lett. **B115**, 242 (1982).
- [12] G. Marchesini, B.R. Webber, G. Abbiendi, I.G. Knowles, M.H. Seymour and L. Stanco, Comp. Phys. Comm. **67**, 465 (1992); G. Corcella, I.G. Knowles, G. Marchesini, S. Moretti, K. Odagiri, P. Richardson, M.H. Seymour, B.R. Webber, preprint hep-ph/9912396.
- [13] T. Sjöstrand, Comput. Phys. Commun. **82**, 74 (1994).
- [14] L. Lönnblad, Comp. Phys. Comm. **71**, 15 (1992).
- [15] H. Baer, F.E. Paige, S.D. Protopopescu and X. Tata, preprint hep-ph/0001086.
- [16] Ya.I. Azimov, Yu.L. Dokshitzer, V.A. Khoze and S.I. Troyan, Phys. Lett. **B165**, 147 (1985); Z. Phys. **27**, 65 (1985).
- [17] D. Amati and G. Veneziano, Phys. Lett. **B83**, 87 (1979); A. Bassetto, M. Ciafaloni and G. Marchesini, Phys. Lett. **83**, 207 (1979); G. Marchesini, L. Trentadue and G. Veneziano, Nucl. Phys. **B181**, 335 (1980).
- [18] B. Anderson, G. Gustafson, G. Ingelman, and T. Sjöstrand, Phys. Rep. **97**, 31 (1983).

- [19] B.R. Webber, Nucl. Phys. **B238**, 492 (1984).
- [20] R.K. Ellis, W.J. Stirling and B.R. Webber, *QCD and Collider Physics*, Cambridge Univ. Press 1996.
- [21] V. Berezinsky, Nucl. Phys. B (Proc. Suppl.) **87**, 387 (2000); P. Bhattacharjee and G. Sigl, Phys. Rep. **327**, 109 (2000).
- [22] V. Berezinsky and M. Kachelrieß, Phys. Lett. **B434**, 61 (1998).
- [23] B.R. Webber, private communication.
- [24] T. Sjöstrand, PYTHIA 5.7 and JETSET 7.4 Physics and Manual, preprint LU TP 95-20 and CERN-TH 7112/93.
- [25] U. Amaldi, W. de Boer and H. Fürstenau, Phys. Lett. **B260**, 447 (1991); J. Ellis, S. Kelly and D.V. Nanopoulos, Phys. Lett. **B260**, 131 (1991).
- [26] S.K. Jones and C.H. Llewellyn-Smith, Nucl. Phys. **B217**, 145 (1983) and references therein.
- [27] P. Langacker and N. Polonsky, Phys. Rev. **D47**, 4028 (1993).
- [28] R. Itoh *et al.* (TOPAZ Collaboration), Phys. Lett. **345B**, 335 (1995); P. Abreu *et al.* (DELPHI Collaboration), Z. Phys. **C73**, 11 (1996); G. Alexander *et al.* (OPAL Collaboration), Z. Phys. **C72**, 191 (1996).
- [29] I.J.D. Craig and J.C. Brown, *Inverse Problems in Astronomy*, Adam Hilger 1986.
- [30] M. Birkel and S. Sarkar, Astrop. Phys. **9**, 297, (1998).
- [31] N.A. Rubin, Master of Philosophy Thesis, University of Cambridge, 1999 (unpublished).
- [32] S. Mrenna, Comput. Phys. Commun. **101**, 232 (1997).
- [33] S. Sarkar, preprint hep-ph/0005256.

splitting channel $i \rightarrow jk$	splitting function $P_{i \rightarrow jk}(z)$
$g \rightarrow g + g$	$3 \left[\frac{z}{1-z} + \frac{1-z}{z} + z(1-z) \right]$
$g \rightarrow \tilde{g} + \tilde{g}$	$3 [z^2 + (1-z)^2]$
$g \rightarrow q + q$	$\frac{n_f^*}{2} [z^2 + (1-z)^2]$
$g \rightarrow \tilde{q} + \tilde{q}$	$3 \{1 - [z^2 + (1-z)^2]\}$
$\tilde{g} \rightarrow g + \tilde{g}$	$3 \frac{1+(1-z)^2}{z}$
$\tilde{g} \rightarrow \tilde{q} + q$	$3 z$
$q \rightarrow q + g$	$\frac{4}{3} \frac{1+z^2}{1-z}$
$q \rightarrow \tilde{q} + \tilde{g}$	$\frac{4}{3} z$
$\tilde{q} \rightarrow \tilde{q} + g$	$\frac{4}{3} \left[\frac{1+z^2}{1-z} - (1-z) \right]$
$\tilde{q} \rightarrow q + \tilde{g}$	$\frac{4}{3}$

Table 1: Splitting functions $P_{i \rightarrow jk}(z)$, where z is the energy fraction of the particle j .

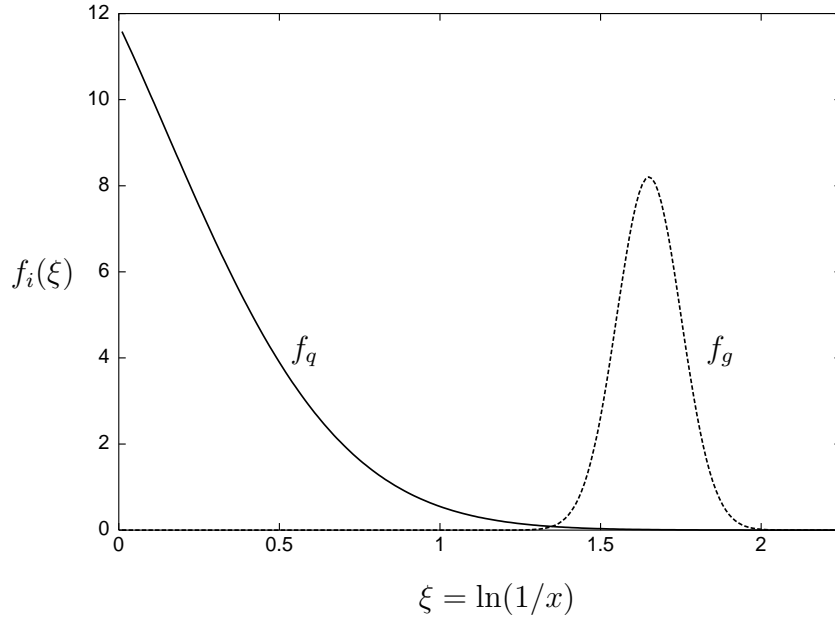


Figure 1: Hadronization functions for quarks $f_q(\xi)$ (solid line) and for gluons $f_g(\xi)$ (broken line) obtained by fitting Gaussians to experimental data at $\sqrt{s} = 91.2$ GeV.

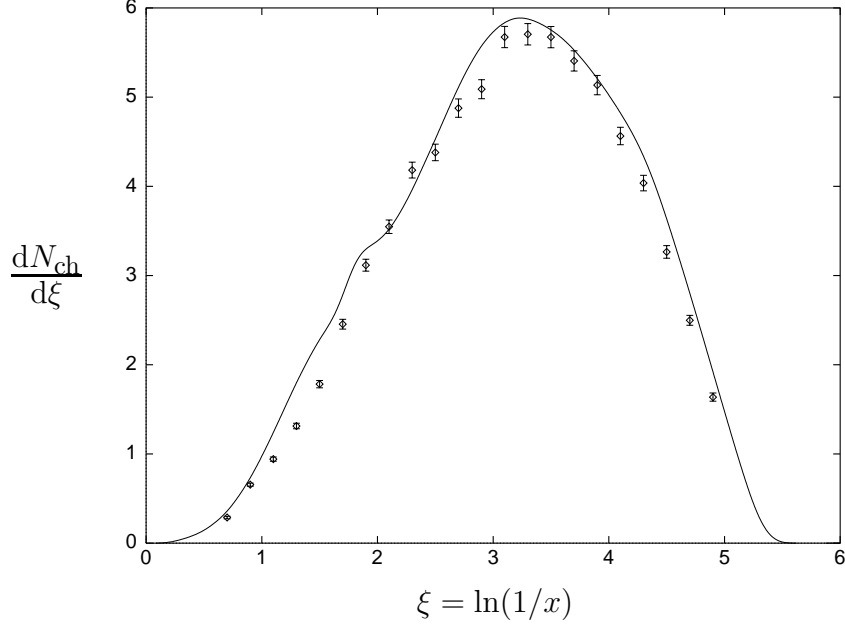


Figure 2: Comparison of the spectrum of charged hadrons $dN_{\text{ch}}/d\xi$ from ordinary QCD Monte Carlo simulation (solid line) with the experimental data (shown with errorbars) at $\sqrt{s} = 58$ GeV.

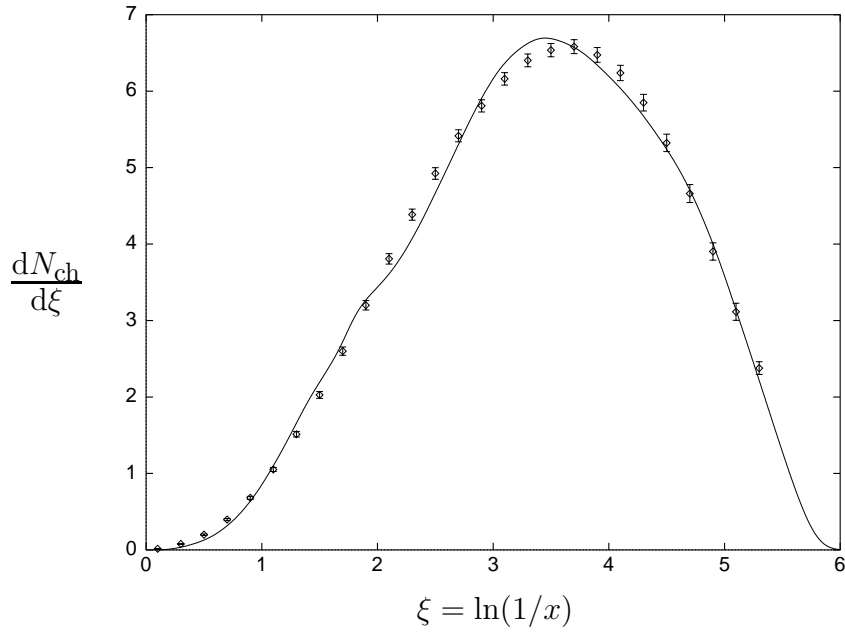


Figure 3: Comparison of the spectrum of charged hadrons $dN_{\text{ch}}/d\xi$ from ordinary QCD Monte Carlo simulation (solid line) with the experimental data (shown with errorbars) at $\sqrt{s} = 91.2$ GeV.

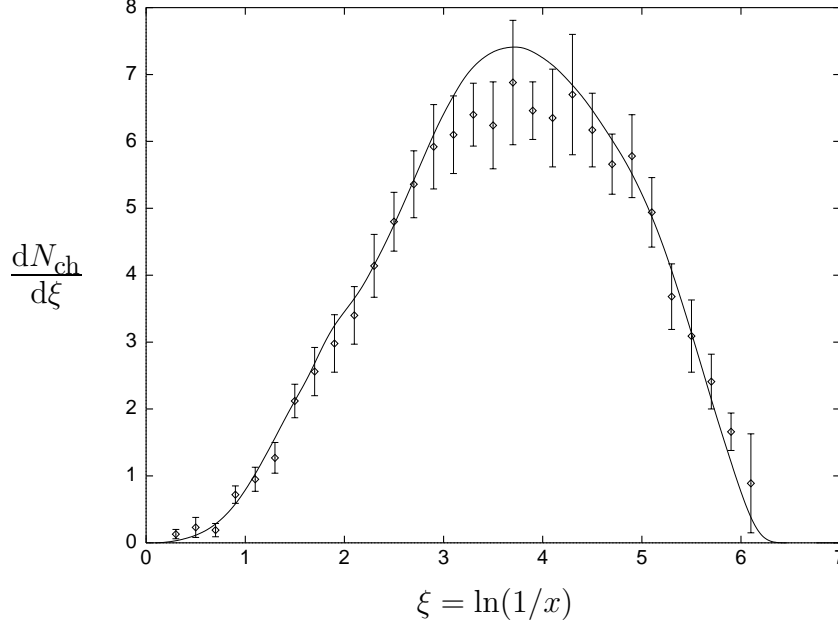


Figure 4: Comparison of the spectrum of charged hadrons $dN_{\text{ch}}/d\xi$ from ordinary QCD Monte Carlo simulation (solid line) with the experimental data (shown with errorbars) at $\sqrt{s} = 133$ GeV.

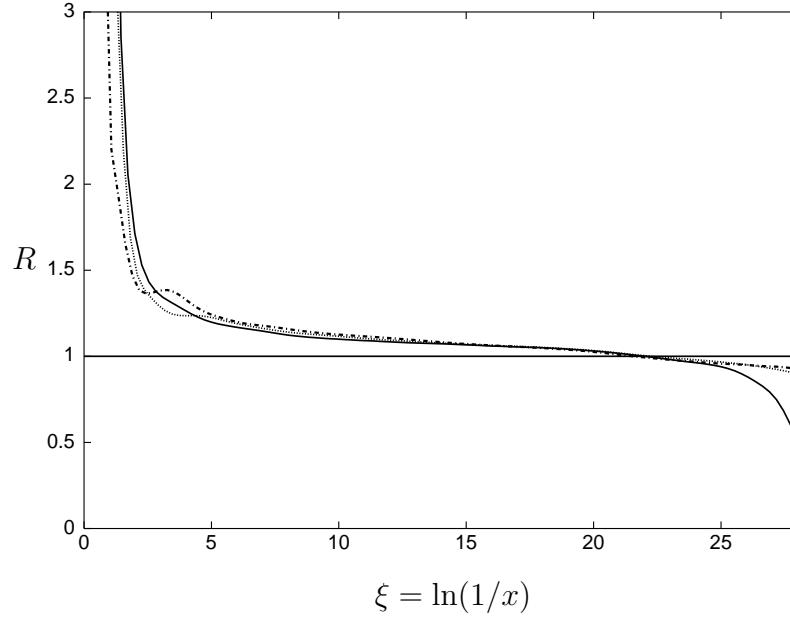


Figure 5: The ratio $R = D_{\text{lim}}(\xi)/D_{\text{MC}}(\xi)$ of the limiting spectrum and of the hadron spectrum from the simulation for $M_X = 10^{12}$ GeV (solid line), 10^{13} GeV (broken line) and 10^{14} GeV (dashed line). All for ordinary QCD with $n_f = 3$.

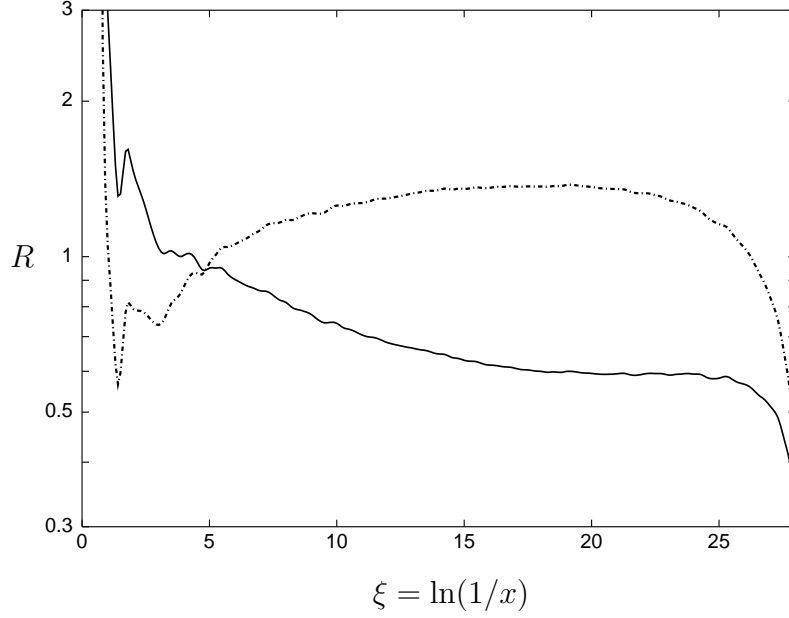


Figure 6: Comparison of the limiting spectrum of QCD for $n_f = 3$ and $n_f = 6$ with the ordinary QCD spectrum from the Monte Carlo simulation: $R = D_{\text{lim}}(\text{QCD}, n_f = 3)/D_{\text{MC}}$ (solid line) and $R = D_{\text{lim}}(\text{QCD}, n_f = 6)/D_{\text{MC}}$ (broken line). Both for $M_X = 10^{12}$ GeV.

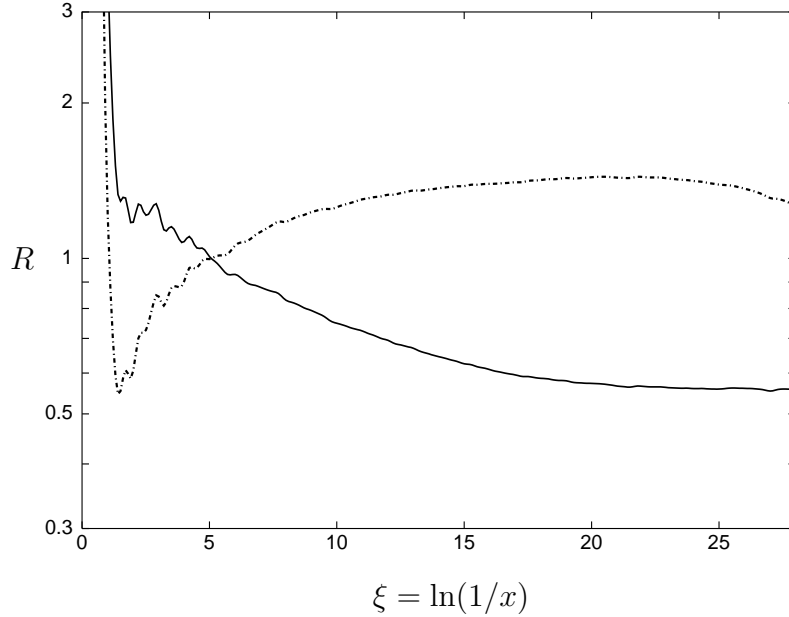


Figure 7: Comparison of the limiting spectrum of QCD for $n_f = 3$ and $n_f = 6$ with the ordinary QCD spectrum from the Monte Carlo simulation: $R = D_{\text{lim}}(\text{QCD}, n_f = 3)/D_{\text{MC}}$ (solid line) and $R = D_{\text{lim}}(\text{QCD}, n_f = 6)/D_{\text{MC}}$ (broken line). Both for $M_X = 10^{14}$ GeV.

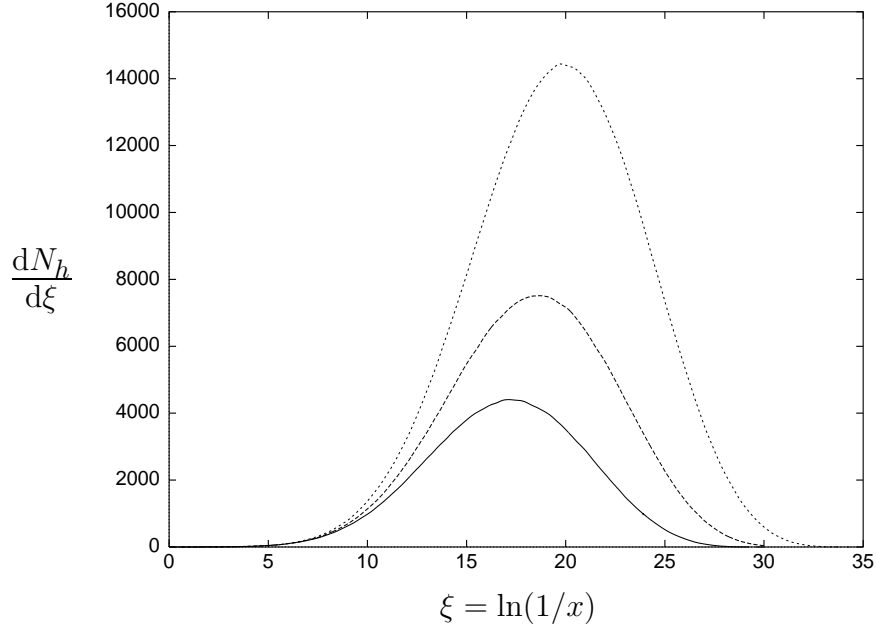


Figure 8: Hadron spectra $dN_h/d\xi$ from SUSY QCD Monte Carlo simulation for $M_X = 10^{12}$ GeV (bottom), $M_X = 10^{13}$ GeV (middle) and $M_X = 10^{14}$ GeV (top), all for $M_{\text{SUSY}} = 200$ GeV.

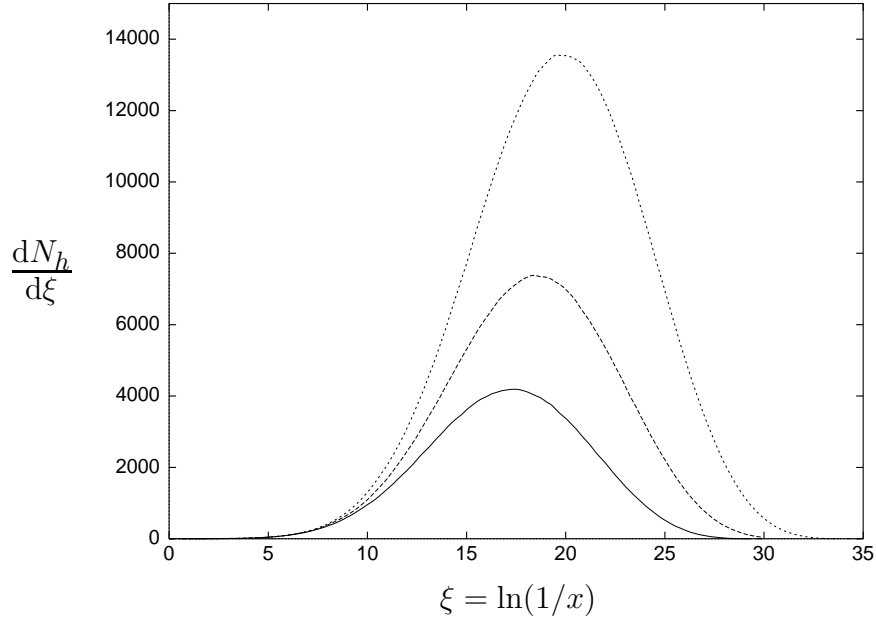


Figure 9: Hadron spectra $dN_h/d\xi$ from SUSY QCD Monte Carlo simulation for $M_X = 10^{12}$ GeV (bottom), $M_X = 10^{13}$ GeV (middle) and $M_X = 10^{14}$ GeV (top), all for $M_{\text{SUSY}} = 1$ TeV.

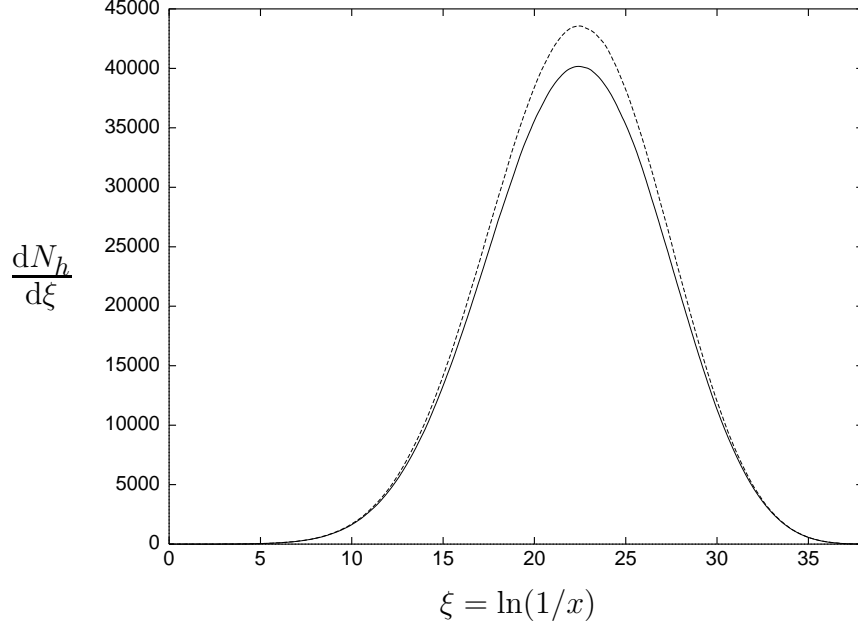


Figure 10: Hadron spectra $dN_h/d\xi$ for SUSY QCD Monte Carlo simulation for $M_{\text{SUSY}} = 200$ GeV (broken line) and $M_{\text{SUSY}} = 1$ TeV (solid line), both for $M_X = 10^{16}$ GeV.

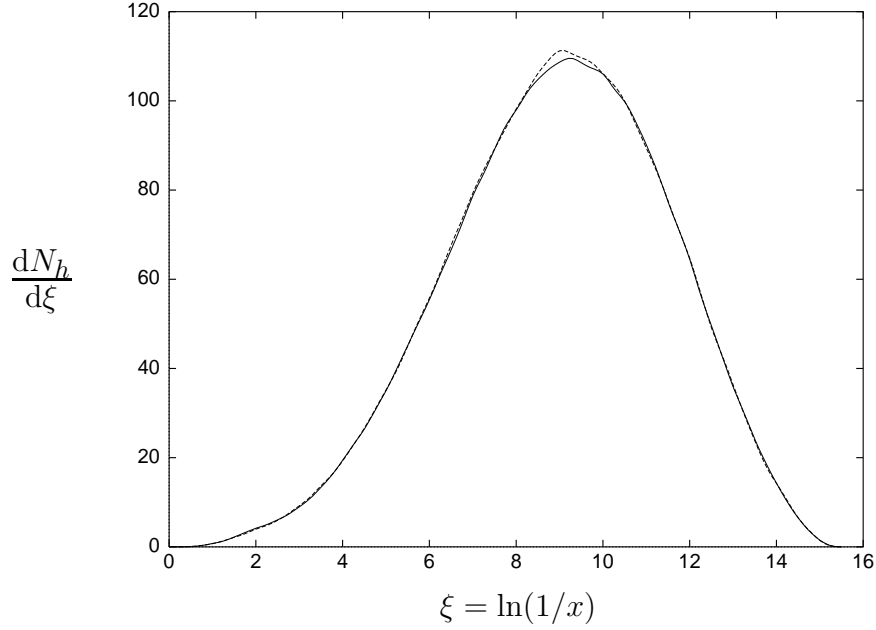


Figure 11: Hadron spectra $dN_h/d\xi$ from SUSY QCD Monte Carlo simulation for $M_{\text{SUSY}} = 200$ GeV (broken line) and $M_{\text{SUSY}} = 1$ TeV (solid line), both for $M_X = 10^6$ GeV.

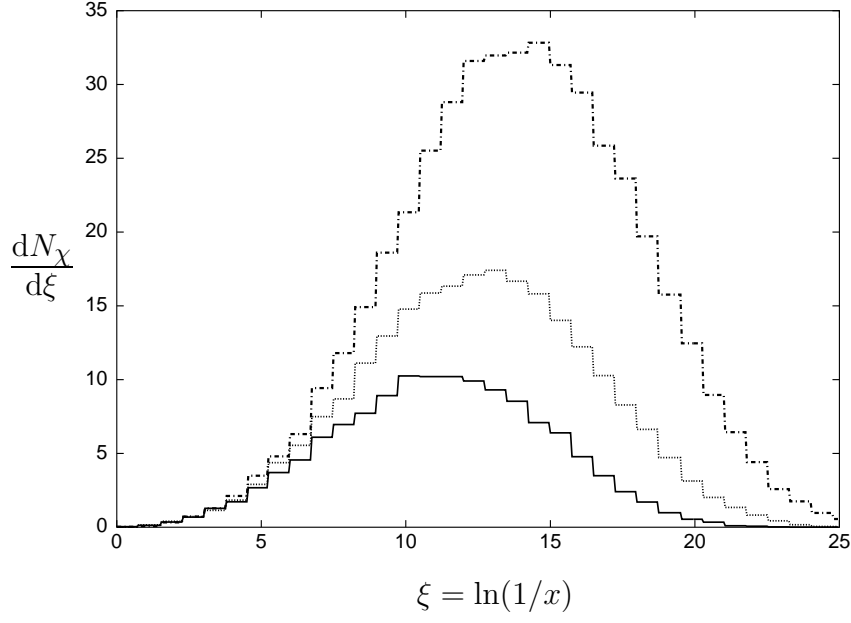


Figure 12: Neutralino spectra from SUSY QCD Monte Carlo simulation for $M_X = 10^{12}$ GeV (bottom), $M_X = 10^{13}$ GeV (middle) and $M_X = 10^{14}$ GeV (top), all for $M_{\text{SUSY}} = 200$ GeV.

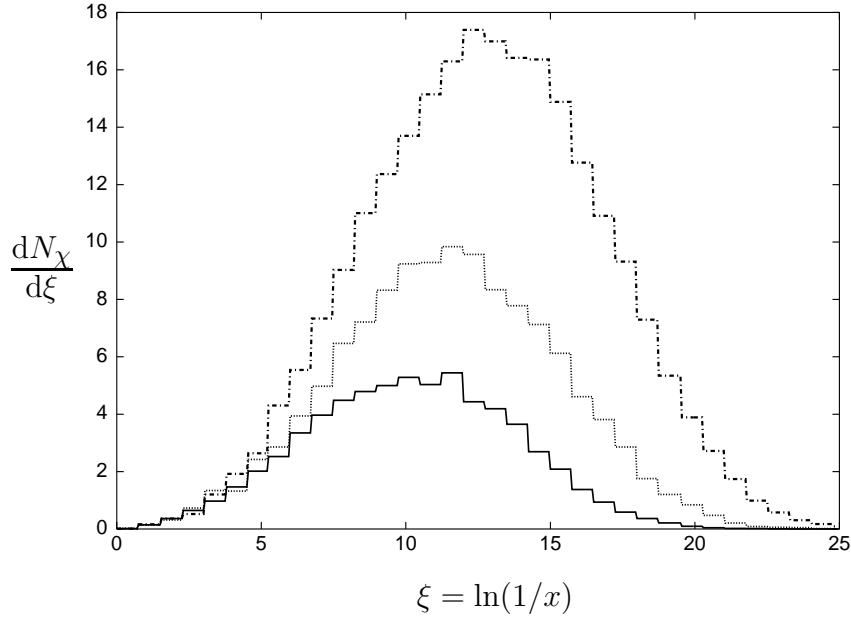


Figure 13: Neutralino spectra from SUSY QCD Monte Carlo simulation for $M_X = 10^{12}$ GeV (bottom), $M_X = 10^{13}$ GeV (middle) and $M_X = 10^{14}$ GeV (top), all for $M_{\text{SUSY}} = 1$ TeV.

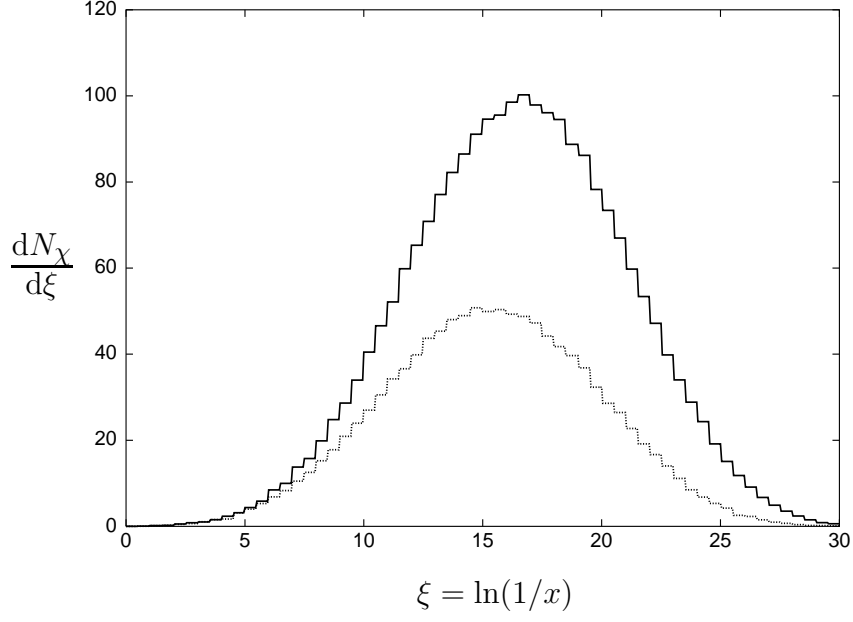


Figure 14: Neutralino spectra from SUSY QCD Monte Carlo simulation for $M_{\text{SUSY}} = 200$ GeV (top) and $M_{\text{SUSY}} = 1$ TeV (bottom), both for $M_X = 10^{16}$ GeV.

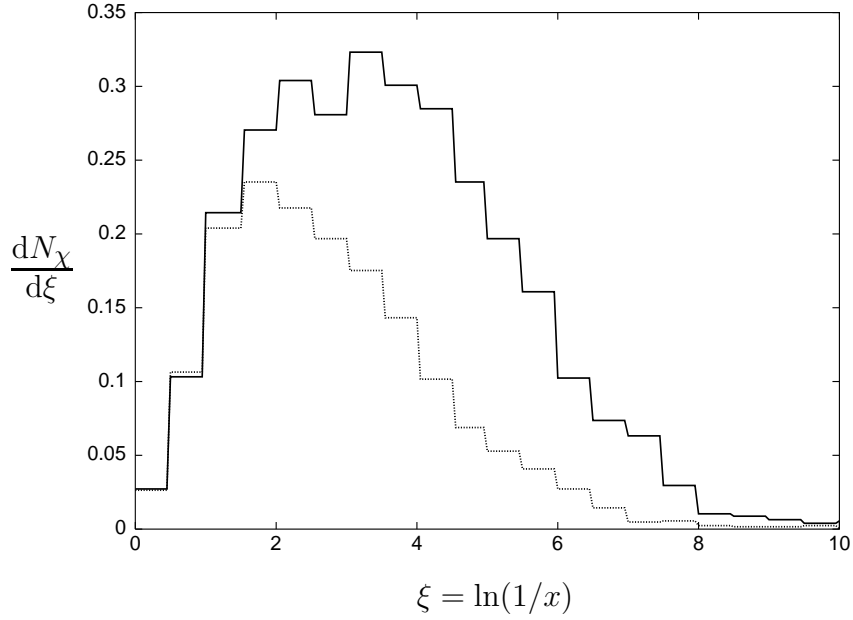


Figure 15: Neutralino spectra from SUSY QCD Monte Carlo simulation for $M_{\text{SUSY}} = 200$ GeV (top) and $M_{\text{SUSY}} = 1$ TeV (bottom), both for $M_X = 10^6$ GeV.

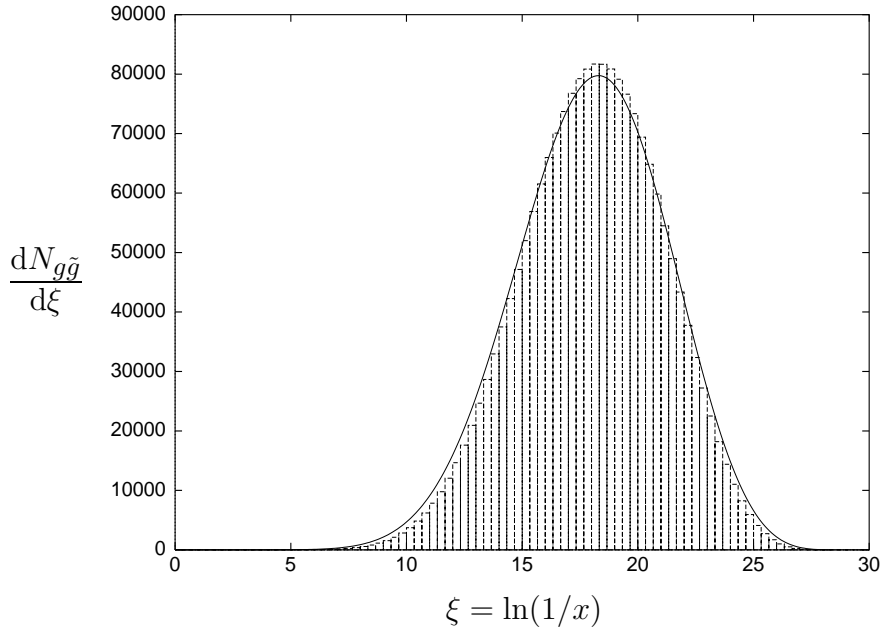


Figure 16: Parton spectrum from SUSY QCD Monte Carlo simulation (boxes) and of the SUSY QCD Limiting Spectrum (solid line) for $M_X = 10^{12}$ GeV. Both for gluons and gluinos only. The coupling constant in the Monte Carlo simulation is frozen at $\tilde{t} < 0.9$ GeV², and $b_s = 3$ is fixed in both cases.

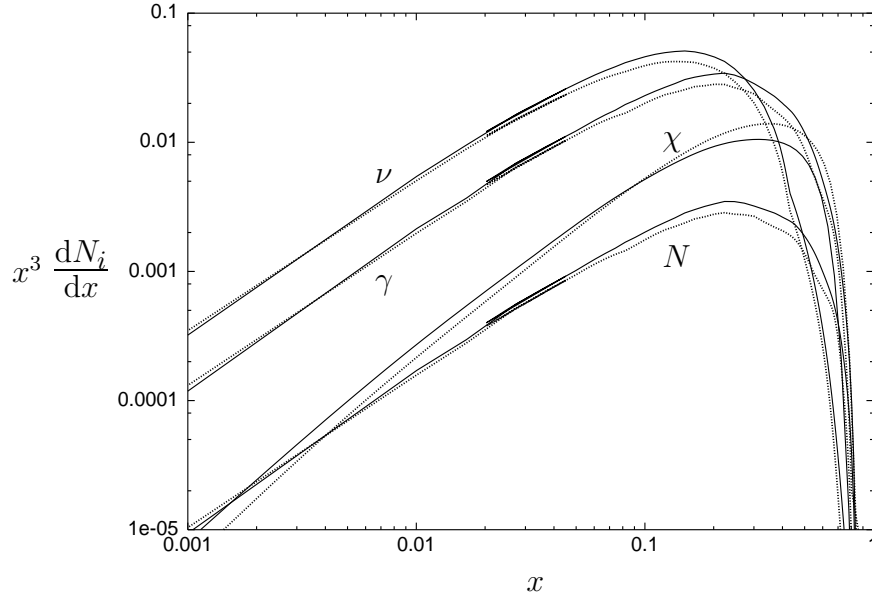


Figure 17: Neutrino, gamma and nucleon fragmentation spectra from SUSY QCD Monte Carlo simulations for $M_X = 10^{12}$ GeV (solid lines) and 10^{14} GeV (dotted lines), all for $M_{\text{SUSY}} = 200$ GeV.